NASA
Technical
Paper
2058

October 1982

Film Thickness Measurement for Spiral Groove and Rayleigh Step Lift Pad Self-Acting Face Seals

Eliseo DiRusso

NASA

NASA Technical Paper 2058

1982

Film Thickness Measurement for Spiral Groove and Rayleigh Step Lift Pad Self-Acting Face Seals

Eliseo DiRusso
Lewis Research Center
Cleveland, Ohio

National Aeronautics and Space Administration

Scientific and Technical Information Branch

Summary

Tests were performed to measure the film thickness (face separation) and seal frictional torque as a function of shaft speed for four self-acting face seal configurations. The self-acting geometries tested were a Rayleigh step lift pad, an outward-pumping spiral groove, and two inward-pumping spiral groove seal configurations. The outside diameter of all the seals was 9.4 cm (3.70 in.). The tests were performed with ambient air at room temperature and atmospheric pressure as the fluid medium. There was no pressure differential across the seals, and the seal face load was a constant 73 N (16.4 lb). The test speed range was 7000 to 17 000 rpm and spanned compressibility numbers from approximately 90 to 400. The tangential velocity at the outside diameter of the seals ranged from 34.5 m/sec (113 ft/sec) at 7000 rpm to 83.7 m/sec (274 ft/sec) at 17 000 rpm. The test results for film thickness were compared with theoretical results from mathematical models (refs. 1 and 2) for calculating film thickness for steady-state conditions.

The tests revealed that the seals operated at a tilt angle (i.e., faces not parallel). The mathematical models for steady-state conditions and parallel faces overpredicted the measured film thickness at the lower speeds of the test speed range and underpredicted the measured film thickness at the higher speeds of the test speed range. The Rayleigh step lift pad configuration displayed fairly steady film thickness measurements, but the three spiral groove configurations displayed a periodic variation in film thickness (squeeze film action) at a frequency approximately four to five times shaft speed. The outward-pumping spiral groove seal tended to be unstable and would not operate at speeds as low as did the Rayleigh step lift pad or the inward-pumping seals.

Introduction

Conventional face seals are very attractive because they have lower leakage rates than labyrinth seals. Conventional rubbing-contact face seals, however, have a pressure differential limit of approximately 90 N/cm^2 (130 psi) and a tangential velocity limit of 122 m/sec (400 ft/sec) for reliable service (ref. 3). By adding a self-acting geometry to one of the faces of the face seal in the form of a Rayleigh step lift pad or spiral grooves, the face seal can be made to operate in a noncontacting mode with approximately 0.0025 to 0.0100 mm (0.0001 to 0.0004 in.) clearance between the faces. This extends the pressure, speed, and life capability of the face seal without leakage penalty (ref. 3, pp. 16-3 and 16-9).

Upon rotation of the shaft the self-acting geometry produces an axial force (lift force) that tends to separate the seal faces. The film thickness (face separation) and its variation with shaft speed and axial force must be known in order to design the face seal for a given face separation and axial force balance. Mathematical models are currently used to calculate lift force and film thickness for various self-acting geometries and seal applications. However, the accuracy of the mathematical models has not been verified by tests.

Tests were performed to measure the film thickness and seal frictional torque for four self-acting seals as a function of speed for a constant seal face load (axial force) of 73 N (16.4 lb). Because the seal face load was fixed by the weight of the shaft, it could not be varied during the tests. The following four self-acting geometries were tested:

(1) Rayleigh step lift pad
(2) Outward-pumping spiral groove
(3) Inward-pumping, deep-groove spiral groove
(4) Inward-pumping, shallow-groove spiral groove

The seals were tested over the speed range 7000 to 17 000 rpm. The tangential velocity at the outside diameter of the seals ranged from 34.5 m/sec (113 ft/sec) at 7000 rpm to 83.7 m/sec (274 ft/sec) at 17 000 rpm. All tests were conducted with ambient air at room temperature and atmospheric pressure as the fluid medium and with no pressure differential across the seals. This minimized the probability of seal distortions due to pressure and temperature. The objectives of the tests were

(1) To experimentally measure the film thickness and seal frictional torque as a function of shaft speed for a constant seal face load

(2) To compare the experimentally measured film thickness with theoretical results from the mathematical models of references 1 and 2.

Apparatus

Seal Test Apparatus

The seal test rig is shown in figure 1. It consisted of a vertically mounted shaft supported radially by two tilting-pad air journal bearings 28 cm (11 in.) apart. The test seal mounted at the lower end of the shaft served as a thrust bearing for the shaft. The shaft was driven by an air turbine (shown in fig. 1) mounted at the top of the rig assembly. Compressed shop air was used to float the tilting-pad air journal bearings and to drive the air turbine.

The test seal assembly shown in figures 2 and 3 consisted of four basic parts:

(1) Seal seat
(2) Primary ring (carbon face seal)
(3) Secondary seal (segmented ring seal)
(4) Carrier

The seal seat was fastened to the shaft by a central nut and rotated with the shaft. The primary ring was retained by the carrier, which fastened to the self-aligning gimbal support shown in figure 3. The secondary seal was required to seal the pneumostatic pressure (discussed below) and was not a test item. The gimbal support permitted the primary ring to align itself with the seal seat. The gimbal support was mounted on a radial air journal bearing and an air thrust bearing as shown in figure 3. These bearings were pressurized with compressed shop air. Further detail on the basic test rig is given in references 4 to 6.

Pneumostatic seal pressurization was provided by compressed shop air ducted through a passage in the seal housing as shown in figure 3. This was used to prevent rubbing of the seal faces during startup and coastdown when the shaft speed was too low to maintain separation of the seal faces. The air pressure required to raise the seal seat clear of the primary ring was 1.52 N/cm^2 (2.2 psig). A pressure transducer was used to monitor the air pressure. The compressed shop air used to drive the turbine, to pressurize the tilting-pad air journal bearings, and to provide pneumostatic seal pressurization was filtered (10 μm) to remove moisture, oil vapor, and solid particles.

Test Seal Configurations

The four self-acting face seal configurations tested were

(1) Rayleigh step lift pad
(2) Outward-pumping spiral groove
(3) Inward-pumping, deep-groove spiral groove
(4) Inward-pumping, shallow-groove spiral groove

The Rayleigh step lift pad primary ring and the seal seat are shown in figure 4. Details of the Rayleigh step lift pad self-acting geometry are shown in figure 5. Note that the self-acting geometry was machined on the surface of the carbon primary ring. The seal seat for this configuration was simply a flat disk. Significant geometric features and dimensions relative to the design of the Rayleigh step lift pad self-acting seal configuration are shown in figure 6.

The outward-pumping spiral groove seal is shown in figure 7. Details of the outward-pumping spiral groove seal self-acting geometry are shown in figure 8(a). The grooves were logarithmic spirals. Figure 8(b) shows details of the primary ring. Note that the self-acting geometry was machined on the seal seat and that the primary ring was a flat surface. This geometry was similar to that used in a seal application for a liquid-oxygen turbopump and was not necessarily an optimized design.

The inward-pumping spiral groove seal is shown in figure 9. Details of the inward-pumping spiral groove seal self-acting geometry are shown in figure 10(a). The grooves were logarithmic spirals. Figure 10(b) shows details of the primary ring. The self-acting geometries for both the deep-groove (0.023 mm, 0.0009 in.) and shallow-groove (0.015 mm, 0.0006 in.) configurations were identical except for the groove depth. Significant geometric features and dimensions relative to the design of the spiral groove self-acting seal configurations are shown in figure 11 for the outward-pumping design and in figure 12 for the inward-pumping design. The inward-pumping, shallow-groove spiral groove seal configuration was an optimized design (i.e., lift force was maximized for this geometry). The computer program of reference 2 was used to optimize the lift force. The parameters that were varied to achieve the optimization were

(1) Spiral groove angle
(2) Groove-to-land width ratio
(3) Groove depth
(4) Number of grooves

The material for all of the seal seats (rotating face) tested was Monel 502. The material for all of the primary rings tested was carbon graphite P692.

Instrumentation

The film thickness between the seal seat and the primary ring was directly measured by three capacitance probes mounted as shown in figures 2 and 3. These probes were equally spaced around the circumference and located at a radius of 5.23 cm (2.06 in.) as shown in figures 5, 8(b), and 10(b). The initial gap between the probes and the seal seat was approximately 0.076 mm (0.003 in.) when the seal seat was contacting the primary ring. The linear measuring range of these probes was 0 to 0.25 mm (0 to 0.010 in.). These three probes were epoxied into the primary ring retainer (figs. 2 and 3) and individually calibrated in a calibration fixture. The film thickness was read out on direct-current voltmeters, recorded on strip-chart recorders, and monitored on oscilloscopes. The resolution was 0.000025 mm (0.000001 in.), and accuracy was estimated to be $\pm$0.0005 mm ($\pm$0.00002 in.).

The axial motion of the seal seat was monitored by three capacitance probes facing the top surface of the seal seat as shown in figure 3. These probes were not exactly 120° apart because of rig space limitations. They were located at a radius of 5.18 cm (2.04 in.). The linear measuring range of these probes was 0 to 0.25 mm (0 to 0.010 in.). These probes were individually calibrated in a calibration fixture and installed in the rig. The film thickness was read out on direct-current voltmeters, recorded on strip-chart recorders, and monitored on oscilloscopes. The resolution was 0.000025 mm

(0.000001 in.), and accuracy was estimated to be ±0.0005 mm (±0.00002 in).

The shaft radial motion at each air journal bearing was monitored by two capacitance probes facing the shaft at each bearing location and mounted normal to each other. These probes are shown schematically in figure 1. This mounting arrangement permitted monitoring the shaft orbit at each air journal bearing to assure safe operation of the rig. These four probes were individually calibrated in a calibration fixture and installed in the rig. The output of these probes was monitored on oscilloscopes.

Shaft speed was sensed by a magnetic speed pickup and automatically controlled to hold any desired speed. The automatic control system varied turbine drive air pressure to maintain the desired speed.

A force transducer was mounted to the gimbal base, which was floated on air bearings as shown in figure 3, such that the transducer measured the tangential force between the gimbal base and ground. This mounting arrangement provided accurate measurement of torque at the seal faces. The force transducer measured tangential force at a radius of 34.9 mm (1.375 in.). The force transducer was calibrated in the rig assembly by using calibrated weights. The force was read out on a direct-current voltmeter and recorded on a strip-chart recorder. The resolution was 0.004 N (0.001 lb), and the accuracy was estimated to be ±0.013 N (±0.003 lb).

Two thermocouples, A and B, located as shown in figure 3 were used to monitor air temperature at the inside radius of the seal and outboard of the seal, respectively.

Procedure

The primary rings and seal seats were lapped flat to within three helium light bands before assembly into the test rig. The lift pad depths and spiral groove depths were inspected and found to be within 0.0025 mm (0.0001 in.) of their nominal values. Before each test run the instrumentation was set up and zeroed with the seal seat resting firmly on the primary ring. The three capacitance probes that measured film thickness had an initial gap of approximately 0.076 mm (0.003 in.) when the gap at the seal faces was zero (zero film thickness). Because the amplifiers were set before each test run to zero out the initial gap, the instrumentation indicated zero when the film thickness was zero. The force transducer was calibrated and zeroed before each run by using calibrated weights. The probes that measured axial shaft motion and the probes that measured shaft orbit were also zeroed before each test.

Prior to starting the turbine drive, the seal seat was raised clear of the primary ring by activating the pneumostatic seal pressurization system. The seal pressure was set at 1.52 N/cm^2 gage (2.2 psig). The shaft was then rotated by hand to assure free rotation without rubbing at the seal faces. The turbine drive was then started and the shaft was slowly accelerated to approximately 14 000 rpm. At this point the pneumostatic seal pressure was gradually reduced while closely monitoring the torquemeter and the three film thickness probes. The torquemeter was used as an indicator of impending contact of the seal faces since the torque would rise rapidly in this situation. The pneumostatic pressure was continually decreased to zero gage pressure. At this point the seal was self-acting and the air film between the seal faces was supporting the weight of the shaft assembly (73 N, 16.4 lb) with a positive clearance. In the event that the torque became unstable or spiked, the pneumostatic pressure was increased to regain stability and a higher speed was selected. The process was then repeated or the test was terminated. Once the seal was self-acting and operating in a stable manner as indicated by the torquemeter, the shaft speed was increased to approximately 17 000 rpm (rig-imposed speed limit) and allowed to stabilize. The data were then recorded. The shaft speed was gradually reduced in approximately 1000-rpm increments while closely monitoring film thickness and the torquemeter. Data were recorded at each speed increment. This process was continued until a speed was encountered at which the torque increased with further decrease in speed. At this point the speed was increased to a point where stable operation was regained.

The speed at which the torque began to increase was identified as the minimum speed for self-acting operation for a given seal. At the completion of the test the shaft speed was set at approximately 14 000 rpm, and the pneumostatic seal pressure was set at 1.52 N/cm^2 gage (2.2 psig). The turbine drive air was then turned off and the shaft was allowed to coast down to a stop. The pneumostatic seal pressure was then reduced to zero. Measurements were recorded after the seal seat was verified to be firmly resting on the primary ring in order to assure that there were no significant zero shifts. This procedure was used for all of the seals tested.

Results and Discussion

A series of tests were conducted to determine the film thickness and frictional torque of one Rayleigh step lift pad configuration and three spiral groove seal configurations for a constant face load of 73 N (16.4 lb) for shaft speeds from 7000 to 17 000 rpm. The tangential velocity at the outside diameter of the seals ranged from 34.5 m/sec (113 ft/sec) at 7000 rpm to to 83.7 m/sec (274 ft/sec) at 17 000 rpm. The compressibility number range was 90 to 400. The compressibility number is defined as

$$\Lambda = \frac{6\mu\omega r^2}{pc^2}$$

where

μ	viscosity
ω	shaft angular velocity
r	seal outside radius
p	pressure at seal boundary
c	film thickness

All of the seals were tested with ambient air at room temperature (21° C, 70° F) and atmospheric pressure (10.1 N/cm^2, 14.7 psia) as the fluid medium. There was no pressure difference across the seal faces. This minimized distortion of the seal faces caused by pressure and temperature loading.

The three probes shown in figure 3 that were used to monitor the seal seat axial motion indicated a periodic axial motion of the seal seat of approximately ±0.0023 mm (±0.00009 in.) at the higher speeds (16 000 rpm) and diminishing to ±0.00102 mm (±0.00004 in.) at the lower speeds (9000 rpm). The frequency of this motion was synchronous with shaft speed. This motion appeared to be a nutation rather than a pure axial translation of the seal seat. The seal seat axial motion was typical for all of the tests. The probes (fig. 1) that monitored the shaft orbits indicated maximum orbit radii of approximately 0.0051 mm (0.0002 in.) throughout the test range. The Rayleigh step lift pad configuration displayed fairly steady film thickness measurements (±0.0013 mm (±0.00005 in.) from the mean value). However, the three spiral groove configurations displayed a periodic variation in film thickness of approximately ±0.0038 mm (±0.00015 in.) at the higher film thicknesses at a frequency approximately four to five times shaft speed.

Rayleigh Step Lift Pad Seal

Figure 13 is a plot of film thickness as a function of shaft speed for the Rayleigh step lift pad seal. The physical location of probes 1, 2, and 3 is shown in figures 2, 3, and 5. At any given speed the steady-state film thicknesses measured at probes 1 and 3 were nearly equal and lower than the film thickness measured at probe 2. This indicates that the seal faces were not running parallel but at a tilt angle (shown schematically in fig. 14). The magnitude of the average tilt angle as calculated from the experimental data was approximately 0.0009° at 16 500 rpm. However, it should be noted that this is an average value. The 0.0009° tilt angle represents a difference in film thickness of 0.0012 mm (0.00005 in.) across the diameter of the seal. Instantaneous values may vary considerably and possibly approach 0.008° at the higher film thicknesses. The dashed curve in figure 13 is a plot of the average of the film thickness measured at probes 1, 2, and 3. The solid curve in figure 13 is a plot of the theoretical film thickness as calculated from a computer program named "RAYTH," which is documented in reference 1. The theoretical curve in figure 13 was calculated for the geometry shown in figure 6 for the physical properties of air at 21° C (70° F) and 10.1 N/cm^2 abs (14.7 psia) and for parallel seal faces. The viscosity used in the computer program was 0.182×10^{-8} N sec/cm^2 (0.264×10^{-8} lbf sec/in^2).

The minimum speed at which this seal would operate in a self-acting mode was 7100 rpm and the maximum speed was 16 500 rpm. The maximum speed was limited by the rig and not by the seal. The minimum speed was identified as the speed at which the torque at the seal face began to increase as the shaft speed was decreased. The increase in torque indicated impending contact of the seal faces, not actual contact. Inspection of the seal faces after completion of the test showed no evidence of rubbing contact. The Rayleigh step lift pad seal ran very smoothly (i.e., torque was very stable throughout the tests and displayed no tendency to spike).

Comparison of the experimental and theoretical results (fig. 13) reveals a significant difference in the slopes of the curves and a crossing of the curves at approximately 14 000 rpm. Below 14 000 rpm the experimentally measured film thickness was lower than the theoretical curve; above 14 000 rpm it was higher. This difference in slopes may in part be due to the tilt angle (discussed above), which was inherent in the tests but was not considered in the theoretical calculation. The tilt angle has the effect of increasing the load capacity (refs. 7 and 8). Hence a seal operating at constant face load and with a tilt angle would produce higher film thickness at any given speed than a seal operating at constant face load and parallel faces. Frictional heating of the film between the seal faces increased with speed during the tests, thereby increasing the fluid viscosity. Higher viscosity would cause higher experimental film thicknesses at higher speeds than the mathematical model predicted since the theoretical data were for a seal operating at 21° C (70° F). This effect, however, was small since the rise in temperature with speed was small. At the lower speeds (approx 7000 rpm) thermocouple A (fig. 3) indicated 27° C (81° F) and thermocouple B indicated 23° C (73° F); at the higher speed (approx 17 000 rpm) thermocouple A indicated 32° C (90° F) and thermocouple B indicated 24° C (76° F). These temperatures were typical for all four of the seals tested.

The experimentally measured average film thickness was below the theoretical film thickness for speeds below approximately 14 000 rpm. This could be caused by distortions of the primary ring and slight deviations in the geometry of the Rayleigh step lift pads from the mean values used in the mathematical model.

Outward-Pumping Spiral Groove Seal

Figure 15 is a plot of film thickness as a function of shaft speed for the outward-pumping spiral groove seal. The physical location of probes 1, 2, and 3 is shown in figures 2, 3, and 8(b). The experimental data show that the seal faces were not running parallel but at a tilt angle shown schematically in figure 14. The magnitude of the average tilt angle as calculated from the experimental data was approximately 0.0009° at 16 500 rpm. However, it should be noted that this is an average value. The 0.0009° tilt angle represents a difference in film thickness of 0.0012 mm (0.00005 in.) across the diameter of the seal. Instantaneous values may vary considerably and possibly approach 0.008° at the higher film thicknesses because of the squeeze film action mentioned previously. The dashed curve in figure 15 is a plot of the average of the film thicknesses measured at probes 1, 2, and 3. The solid curve in figure 15 is a plot of the theoretical film thickness as calculated from the computer program of reference 2. The theoretical curve in figure 15 was calculated for the spiral groove geometry shown in figure 11 and for the physical properties of air at 21° C (70° F) and 10.1 N/cm^2 abs (14.7 psia) and for parallel seal faces. The viscosity used in the computer program was 0.182×10^{-8} N/cm^2 (0.264×10^{-8} lbf sec/in^2).

The minimum speed at which this seal would operate in a self-acting mode was 11 600 rpm, and the maximum speed was 16 500 rpm. The maximum speed was limited by the rig and not by the seal. This seal showed evidence of rubbing contact, which occurred at approximately 11 600 rpm. Below this speed the torquemeter displayed a sustained increase in force, an indication of rubbing contact. Figures 16(a) and (b) show the primary ring and seal seat, respectively, after testing. During the rub, carbon dust was pumped toward the outside of the grooves, where it accumulated and caused a heavy circumferential wear pattern in the carbon (primary ring), as indicated in figure 16(a). The accumulation of carbon dust in the spiral grooves is shown in figure 16(b).

The outward-pumping spiral groove seal was prone to rubbing and would not operate at speeds as low the Rayleigh step lift pad seal or the inward-pumping seals. Also, as the minimum speed for self-acting operation was approached, the seal tended to rub without warning and the torque spiked erratically. All of the other seals approached the minimum speed for self-acting operation very predictably with a gradual increase in torque. The erratic behavior can be explained in part by a potential distortion of the primary ring resulting from the pressure distribution induced by the spiral groove lift force. The pressure distribution on the primary ring (shown schematically in fig. 17(a)) caused a diverging coning angle with respect to the flow direction for the outward-pumping spiral groove seal and hence an unstable condition. Calculation of the coning angle revealed a potential maximum angle of 0.016° for the outward-pumping seal. This angle would cause a divergence of approximately 0.0025 mm (0.0001 in.) over the radial length of the seal face. For the inward-pumping spiral groove seal a converging coning angle (shown schematically in fig. 17(b)) was formed with respect to the flow direction, resulting in a stable condition. The coning angle for the inward-pumping seals was less than that for the outward-pumping seal because the center of pressure was closer to the reaction point (fig. 17). The effects of various distortions are discussed in references 3 to 12. Reference 13 discusses the the fact that negative pressures are generated in outward-pumping spiral groove bearings when the seal band radius approaches the outside radius (fig. 11). This may also contribute to the instability of the outward-pumping spiral groove seal.

Inward-Pumping, Deep-Groove Spiral Groove Seal

Figure 18 is a plot of film thickness as a function of shaft speed for the inward-pumping spiral groove seal with 0.023-mm (0.0009-in.) groove depth. The physical location of probes 1, 2, and 3 is shown in figures 2, 3, and 10(b). The dashed curve in figure 18 is a plot of the average of the film thicknesses measured at probes 1, 2, and 3. The solid curve in figure 18 is a plot of the theoretical film thickness as calculated from the computer program of reference 2. The theoretical curve in figure 18 was calculated for the geometry shown in figure 12 for the physical properties of air at 21° C (70° F) and 10.1 N/cm^2 abs (14.7 psia) and for parallel seal faces. The viscosity used in the computer program was 0.182×10^{-8} N sec/cm^2 (0.264×10^{-8} lbf sec/in^2).

The experimental data show that the seal faces were operating with a tilt angle. However, the angle was considerably less than for the Rayleigh step lift pad or outward-pumping spiral groove seals. The test data for the inward-pumping, deep-groove seal agreed much more closely with the mathematical model. This was probably because the tilt angle was small and the seal faces were nearly parallel.

The minimum speed at which the inward-pumping, deep-groove spiral groove seal would operate in a self-acting mode was 12 800 rpm, and the maximum speed was 17 100 rpm. The maximum speed was limited by the rig and not by the seal. The seal ran smoothly, but the torquemeter indicated rather erratic changes in torque at the lower speed (12 800 rpm). Inspection of the seal faces after completion of the test showed some evidence of rubbing (slight circumferential streaking of the carbon). This probably occurred when the seal was operating near its lowest speed for self-acting operation (12 800 rpm).

Inward-Pumping, Shallow-Groove Spiral Groove Seal

Figure 19 is a plot of film thickness as a function of shaft speed for the inward-pumping spiral groove seal with 0.015-mm (0.0006-in.) groove depth. The physical location of probes 1, 2, and 3 is shown in figures 2, 3, and 10(b). The film thicknesses measured at probes 2 and 3 were nearly equal and higher than that measured at probe 1. This indicates that the seal was operating at a tilt angle. The magnitude of the average tilt angle as calculated from the experimental data was approximately 0.0015° at 17 000 rpm. However, it should be noted that this is an average value. The 0.0015° tilt angle represents a difference in film thickness of 0.0020 mm (0.00008 in.) across the diameter of the seal. Instantaneous values may vary considerably and possibly approach 0.01° because of the squeeze film action mentioned previously. The dashed curve in figure 19 shows the average of the three probes at any given speed. The solid curve in figure 19 shows theoretical results from the computer program of reference 2. The theoretical curve in figure 19 was calculated for the geometry shown in figure 12 for the physical properties of air at 21° C (70° F) and 10.1 N/cm^2 abs (14.7 psia) and for parallel seal faces. The viscosity used in the computer program was 0.182×10^{-8} N sec/cm^2 (0.264×10^{-8} lbf sec/in^2).

The minimum speed for self-acting operation was approximately 7000 rpm. The maximum speed of 17 000 rpm was limited by the rig and not by the seal. Inspection of the seal faces after completion of the test showed no evidence of rubbing contact. The inward-pumping, shallow-groove spiral groove seal ran very smoothly (i.e., the torquemeter was very stable throughout the test and displayed no tendency to spike).

Comparative Results

Figure 20 is a comparison of measured film thicknesses as a function of shaft speed for the four seals tested. The Rayleigh step lift pad, outward-pumping spiral groove, and inward-pumping, deep-groove spiral groove seals were comparable in average film thickness. However, the inward-pumping, shallow-groove spiral groove seal showed significantly higher film thickness (approx 40 percent higher at 14 000 rpm) than the other three seals. It should be noted that the inward-pumping, shallow-groove spiral groove seal configuration was an optimized design (i.e., lift force was maximized for this geometry).

Figure 21 is a comparison of the experimentally measured seal frictional torque as a function of shaft speed for the four seals tested. The experimentally measured seal frictional torque for the inward-pumping, shallow-groove spiral groove seal showed a linear increase with speed between 7000 and 13 000 rpm, terminating in a plateau at speeds above 13 000 rpm. No explanation is offered for this phenomenon. The three spiral groove configurations showed seal frictional torques that were comparable to those for the Rayleigh step lift pad seal at speeds above approximately 13 000 rpm and approximately 56 percent higher at 14 000 rpm. The higher torque of the spiral groove configurations may be partially due to the squeeze film action displayed by these seals.

Summary of Results

The film thickness and seal frictional torque for self-acting face seals were experimentally measured as a function of shaft speed for four self-acting geometries. The seals were tested with air at room temperature and atmospheric pressure as the fluid medium and with no pressure differential across the seals. The four self-acting geometries tested were

(1) Rayleigh step lift pad
(2) Outward-pumping spiral groove
(3) Inward-pumping, deep-groove spiral groove
(4) Inward-pumping, shallow-groove spiral groove

All of the seals had an outside diameter of 9.4 cm (3.70 in.). The seals were tested over a speed range from 7000 to 17 000 rpm for a constant face load of 73 N (16.4 lb). The tangential velocity at the outside diameter of the seals ranged from 34.5 m/sec (113 ft/sec) at 7000 rpm to 83.7 m/sec (274 ft/sec) at 17 000 rpm. The measured film thickness was compared to mathematical models for calculating film thickness. The theoretical results from the mathematical models were for steady film thickness (i.e., no squeeze film action), parallel seal faces, and fluid properties of air at 21° C (70° F) and atmospheric pressure (10.1 N/cm^2 abs, 14.7 psia).

The tests revealed the following:

1. At the lower speeds of the test speed range the mathematical models overpredicted the measured film thickness, and at the higher speeds of the test speed range the mathematical models underpredicted the measured film thickness. This is partially attributed to tilt angle and fluid film heating, which were not considered in the mathematical models.

2. The inward-pumping, shallow-groove spiral groove seal had approximately 40 percent higher measured film thickness at 14 000 rpm than the other three seals tested. This was an optimized design (i.e., lift force was maximized for this geometry).

3. The relative smoothness of operation of the four seals (listed in decreasing order of smoothness) was Rayleigh step lift pad; inward-pumping, shallow-groove spiral groove; inward-pumping, deep-groove spiral groove; and outward-pumping spiral groove. (The outward-pumping seal tended to be unstable.)

4. The minimum speed for self-acting operation for

the Rayleigh step lift pad seal and the inward-pumping, shallow-groove spiral groove seal was 7000 rpm; the minimum speed for the outward-pumping spiral groove seal was 11 700 rpm; the minimum speed for the inward-pumping, deep-groove spiral groove seal was 12 700 rpm.

5. The measured film thickness for the Rayleigh step lift pad seal was fairly steady (± 0.0013 mm (0.00005 in.) from the mean value). However, the spiral groove seal configurations displayed a periodic variation in film thickness of approximately ± 0.0038 mm (± 0.00015 in.) at the higher film thicknesses at a frequency approximately four to five times shaft speed.

6. The seals operated with a tilt angle (i.e., seal faces not parallel). The potential extreme value for tilt angle was calculated to be 0.01° for the inward-pumping, shallow-groove seal.

7. The Rayleigh step lift pad seal had 36 percent less frictional torque at 14 000 rpm than the three spiral groove seals tested.

Lewis Research Center
National Aeronautics and Space Administration
Cleveland, Ohio, March 30, 1982

References

1. Zuk, J.; Ludwig, L. P; and Johnson, R. L.: Design Study Of Shaft Face Seal with Self-Acting Lift Augmentation. I – Self-Acting Pad Geometry. NASA TN D-5744, 1970.
2. Mechanical Engineering Laboratory of The Franklin Research Center, A Division of The Franklin Institute: Spiral Groove Face Seal Computer Program (SEALSG). Franklin Research Center Project Number 21464, Mar. 1979.
3. Ludwig, L. P.: Self-Acting Shaft Seals. NASA TM-73856, 1978.
4. Nemeth, Z. N.; and Anderson, W. J.: Dynamic Behavior of Air-Lubricated Pivoted-Pad Journal Bearing Rotor System. I – Effects of Mount Stiffness and Damping. NASA TN D-5685, 1970.
5. Nemeth, Z. N.: Dynamic Behavior of Air-Lubricated Pivoted-Pad Journal Bearing Rotor System. II – Pivot Consideration and Pad Mass. NASA TN D-6606, 1972.
6. Nemeth, Z. N.: Operating Characteristics of a Cantilever-Mounted Resilient-Pad Gas-Lubricated Thrust Bearing. NASA TP-1438, 1979.
7. Colsher, R.; and Shapiro, W.: Steady-State and Dynamic Performance of a Gas-Lubricated Seal. (F-C3452-1, Franklin Institute Research Labs; NAS3-16863.) NASA CR-121093, 1972.
8. Haardt, R.; and Godet, M.: Axial Vibration of a Misaligned Radial Face Seal, Under a Constant Closure Force. ASLE Trans., vol. 18, no. 1, May 1974, pp. 55-61.
9. Johnson, R. L.; and Ludwig, L. P.: Shaft Face Seal with Self-Acting Lift Augmentation for Advanced Gas Turbine Engines. NASA TN D-5170, 1969.
10. Cheng, H. S.; Chow, C. Y.; and Wilcock, D. F.: Behavior of Hydrostatic and Hydrodynamic Noncontacting Face Seals. J. Lubr. Technol., vol. 90, no. 2, Apr. 1968, pp. 510-519.
11. Ludwig, L. P.: Face-Seal Lubrication. I – Proposed and Published Models. NASA TN D-8101, 1976.
12. Ludwig, L. P.; and Allen, G. P.: Face-Seal Lubrication. II – Theory of Response to Angular Misalignment. NASA TN D-8102, 1976.
13. Muijderman, E. A.: Spiral Groove Bearings. Philips Technical Library, 1966.

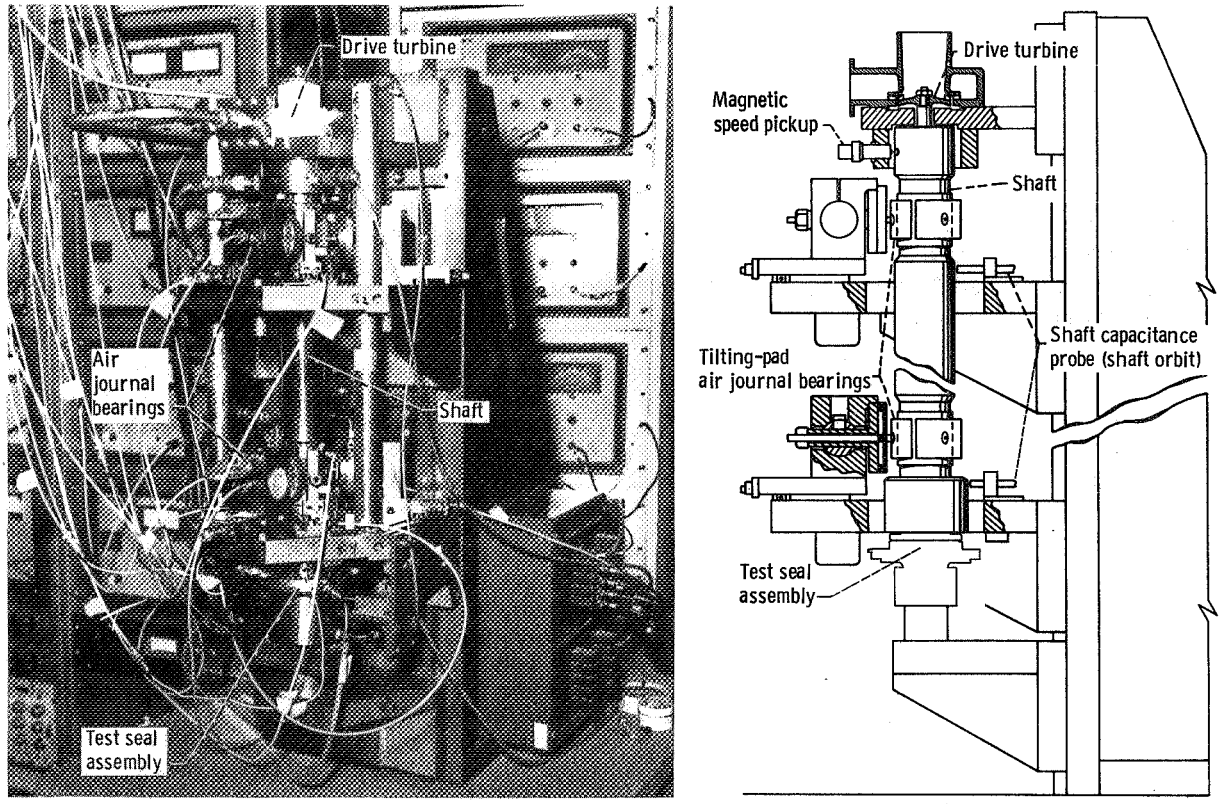

Figure 1. - Seal test apparatus.

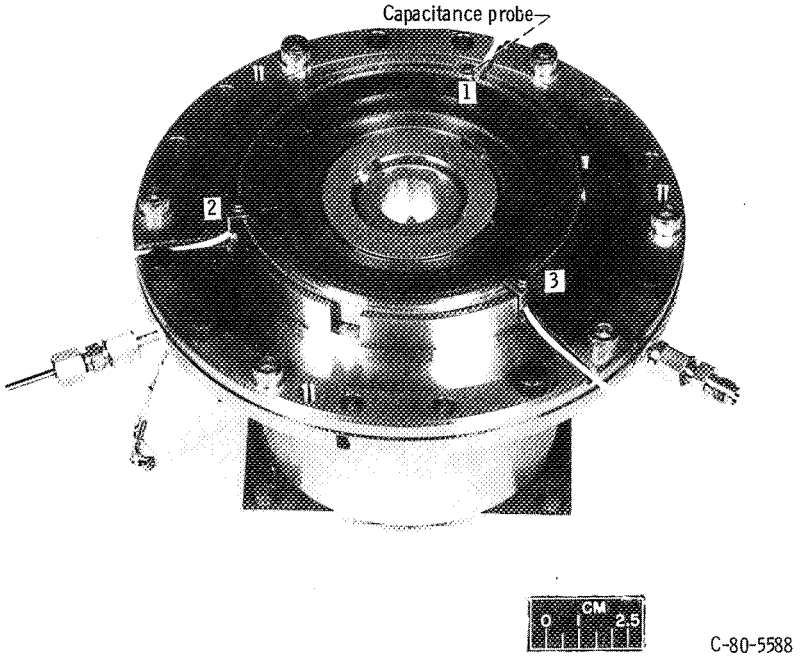

C-80-5588

Figure 2. - Seal assembly (Rayleigh step lift pad seal shown).

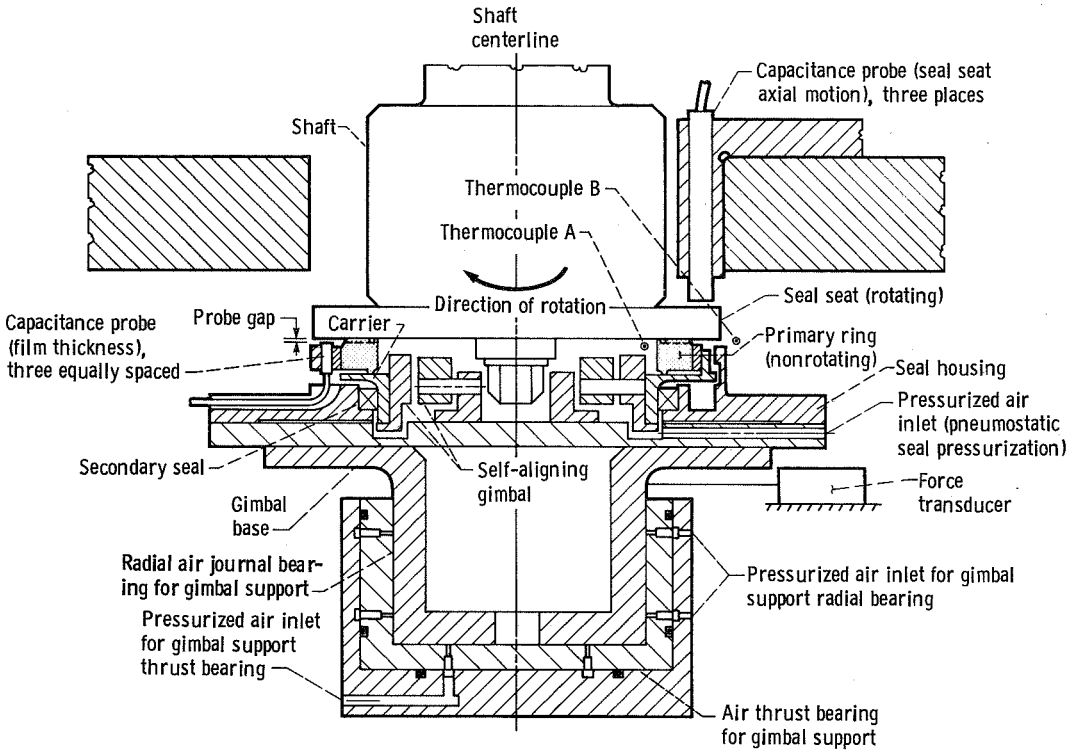

Figure 3. - Schematic of seal assembly and self-aligning gimbal support.

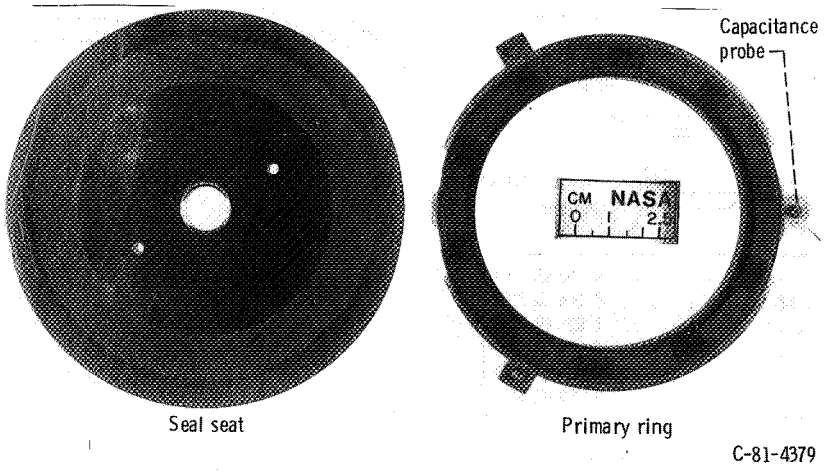

Figure 4. - Rayleigh step lift pad seal.

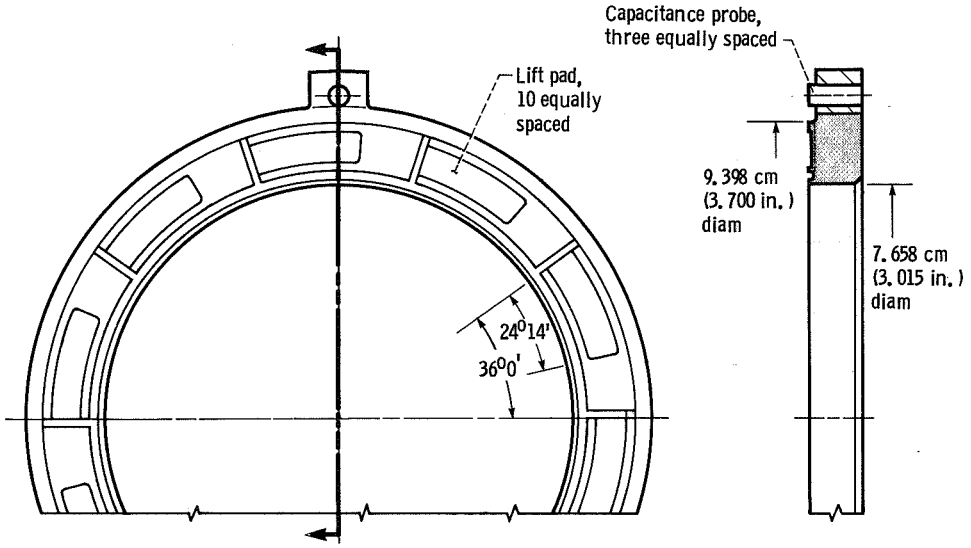

Figure 5. - Details of Rayleigh step lift pad primary ring.

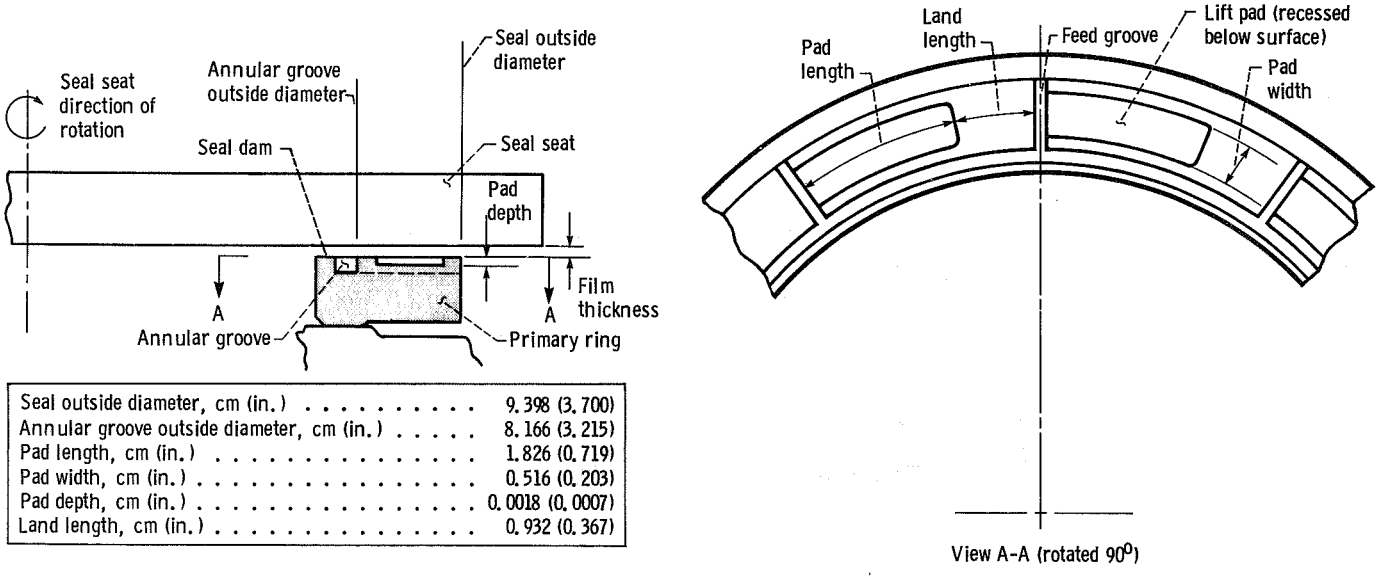

Seal outside diameter, cm (in.)	9.398 (3.700)
Annular groove outside diameter, cm (in.)	8.166 (3.215)
Pad length, cm (in.)	1.826 (0.719)
Pad width, cm (in.)	0.516 (0.203)
Pad depth, cm (in.)	0.0018 (0.0007)
Land length, cm (in.)	0.932 (0.367)

Figure 6. - Raleigh step lift pad - significant geometric features and dimensions.

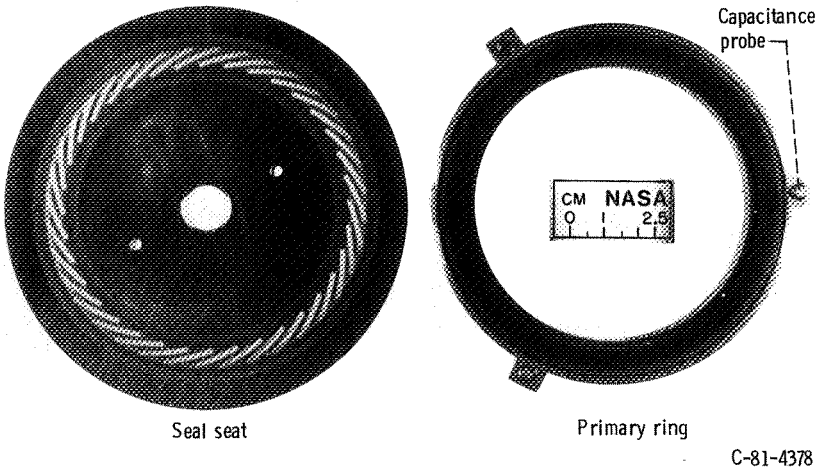

Figure 7. - Outward-pumping spiral groove seal.

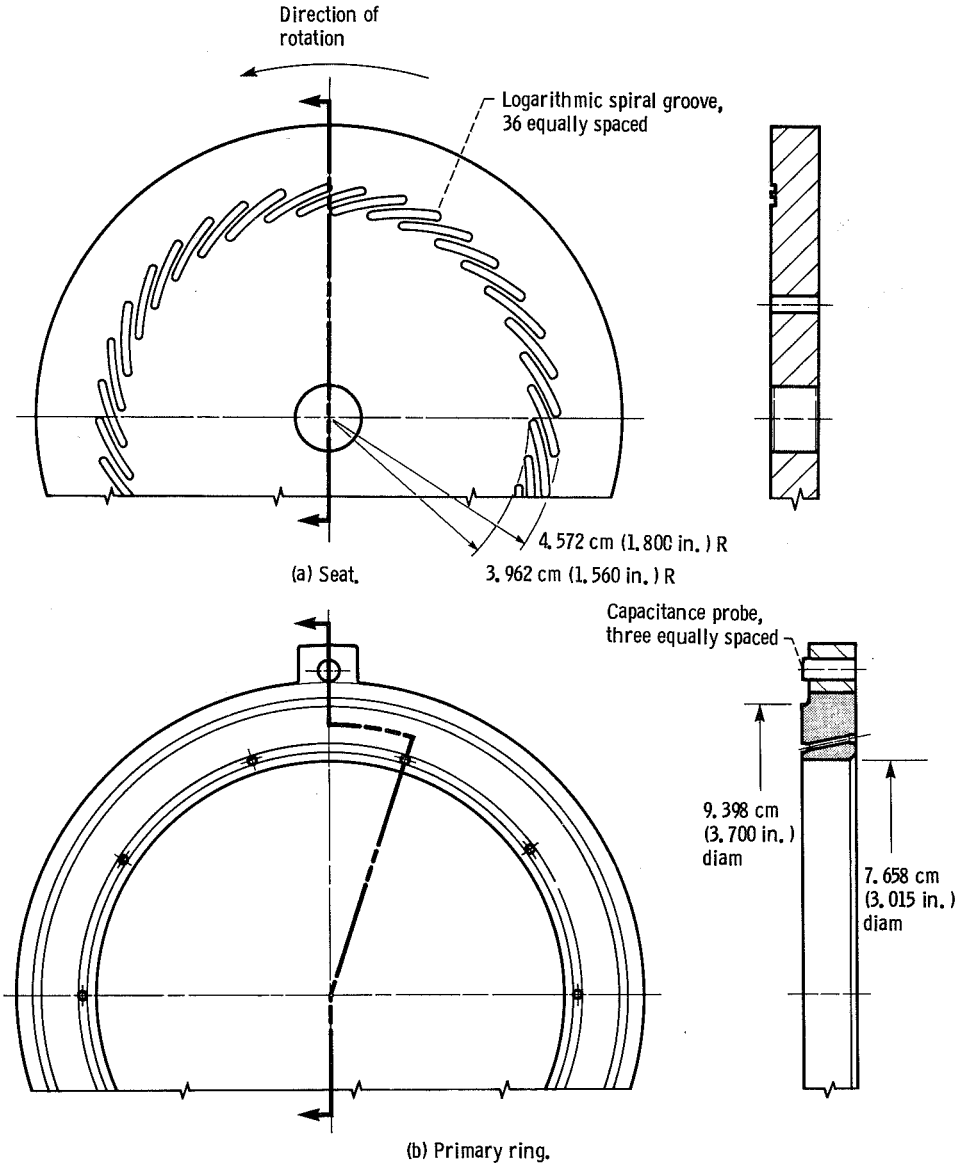

Figure 8. - Details of outward-pumping spiral groove seal.

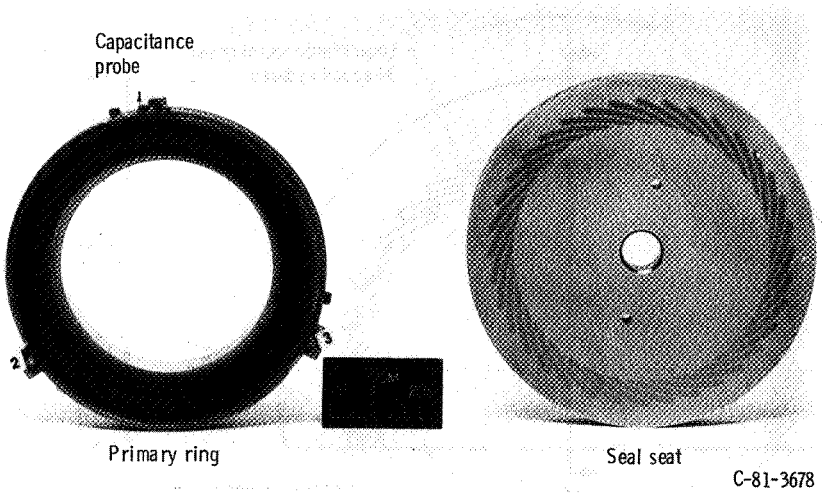

Figure 9. - Inward-pumping spiral groove seal.

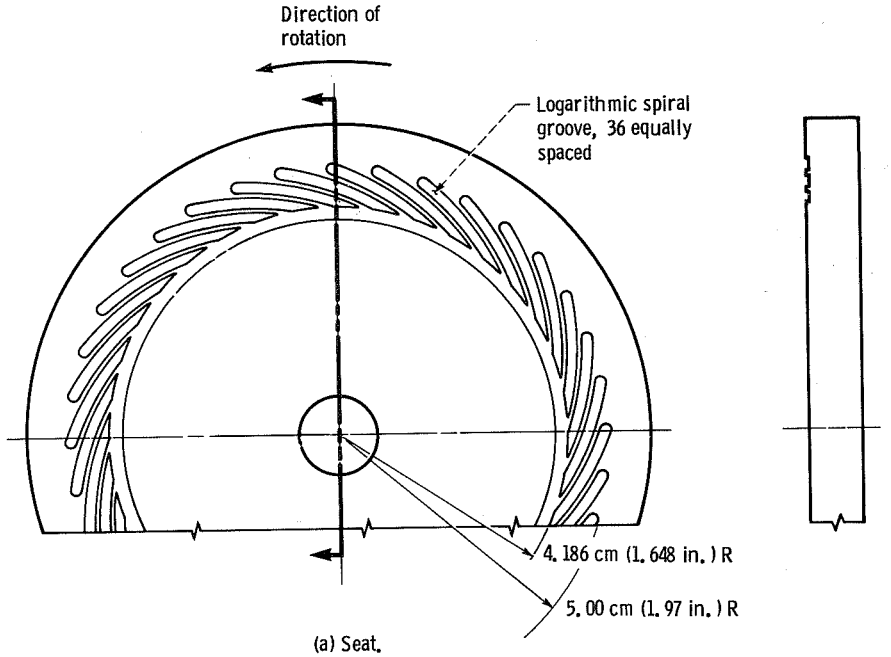

(a) Seat.

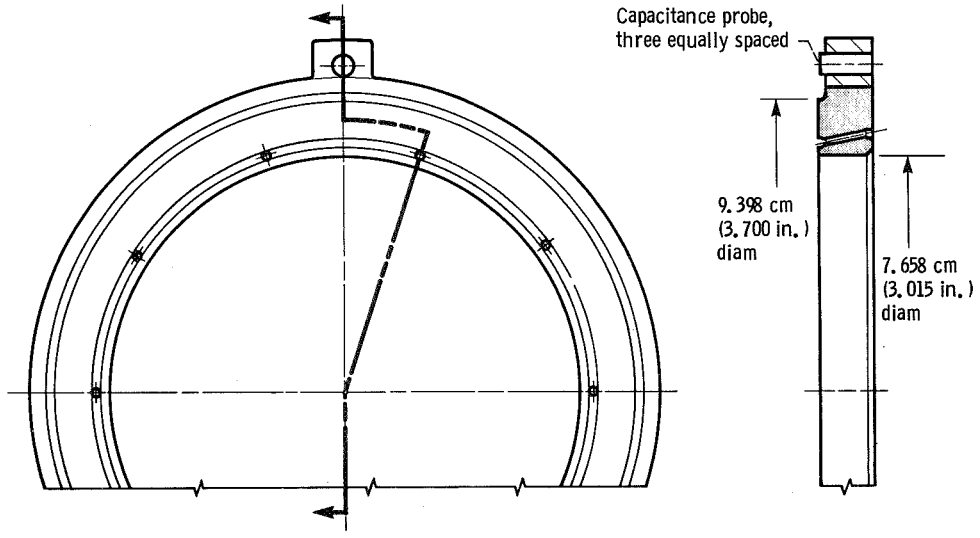

(b) Primary ring.

Figure 10. - Details of inward-pumping spiral groove seal seat.

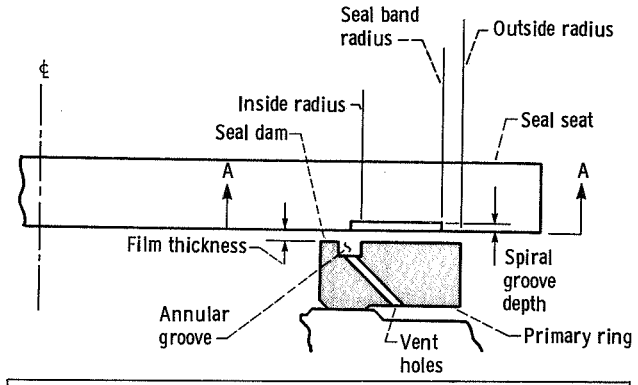

Outside radius, cm (in.)	4.699 (1.850)
Inside radius, cm (in.)	4.084 (1.608)
Seal band radius, cm (in.)	4.572 (1.800)
Spiral groove depth, cm (in.)	0.0018 (0.0007)
Groove width (measured circumferentially), cm (in.)	0.455 (0.179)
Land width (measured circumferentially), cm (in.)	0.279 (0.110)
Groove-to-land width ratio	1.63
Spiral groove angle, deg	20

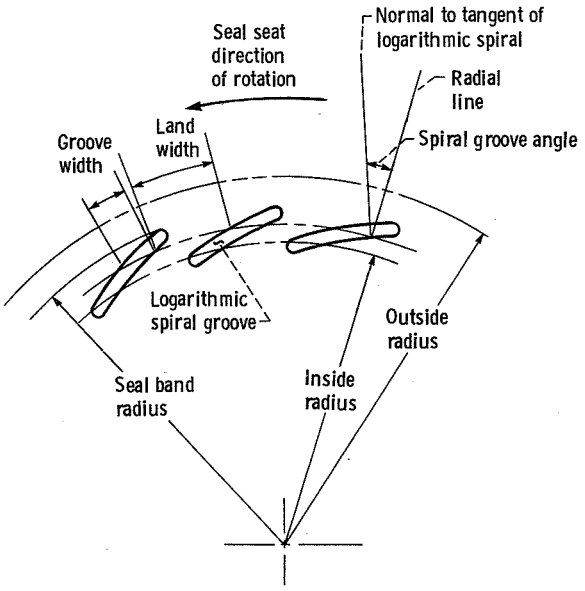

View A-A (rotated 90°, not to scale)

Figure 11. - Outward-pumping spiral groove seal - significant geometric features and dimensions.

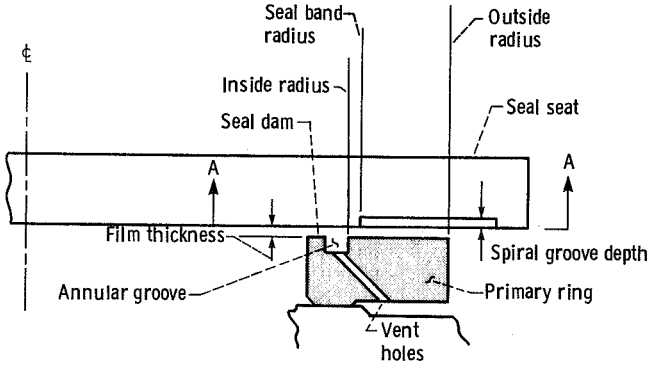

Outside radius, cm (in.)	4.699 (1.850)
Inside radius, cm (in.)	4.084 (1.608)
Seal band radius, cm (in.)	4.186 (1.648)
Spiral groove depth, cm (in.):	
Shallow groove	0.0015 (0.0006)
Deep groove	0.0023 (0.0009)
Groove width (measured circumferentially, cm (in.)	0.549 (0.216)
Land width (measured circumferentially, cm (in.)	0.229 (0.090)
Groove-to-land width ratio	2.40
Spiral groove angle, deg	20

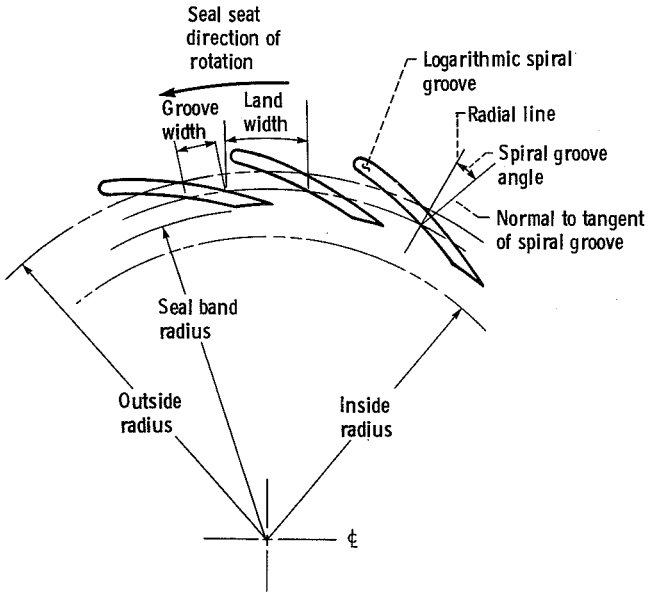

View A-A (rotated 90°, not to scale)

Figure 12. - Inward-pumping spiral groove seal - significant geometric features and dimensions.

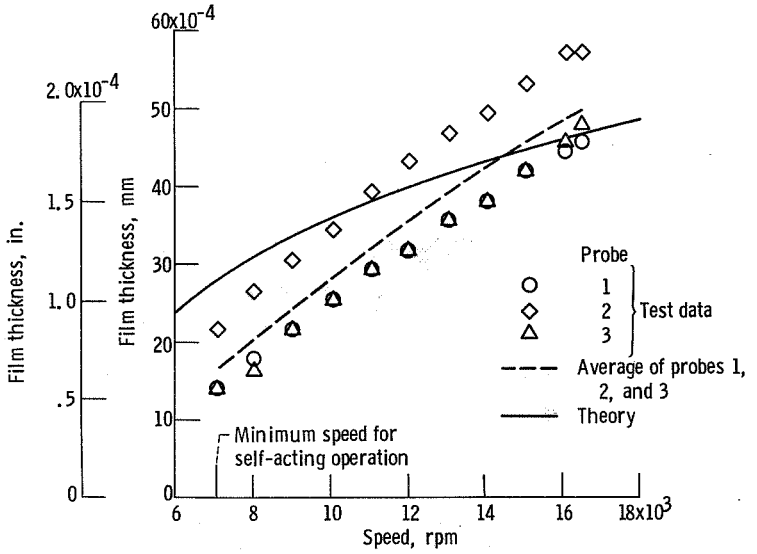

Figure 13. - Film thickness as function of shaft speed - comparison of test data with theory for Rayleigh step lift pad. Seal face load, 73 N (16.4 lb).

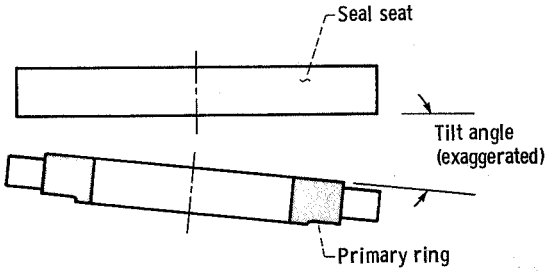

Figure 14. - Schematic showing face seal tilt angle.

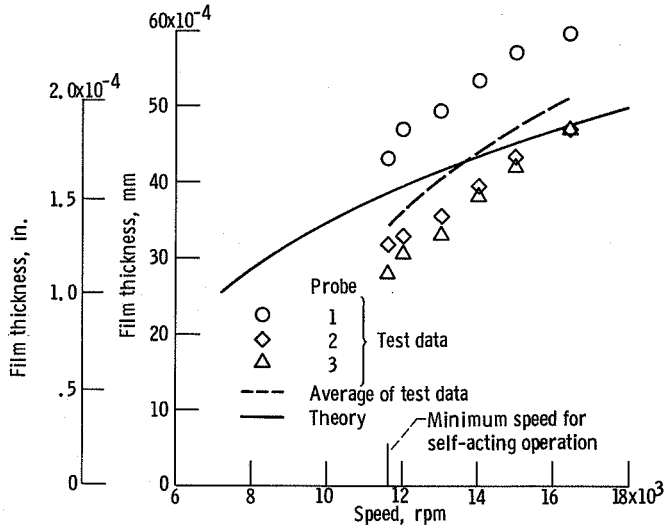

Figure 15. - Film thickness as function of shaft speed - comparison of test data with theory for outward-pumping spiral groove. Seal face load, 73 N (16.4 lb).

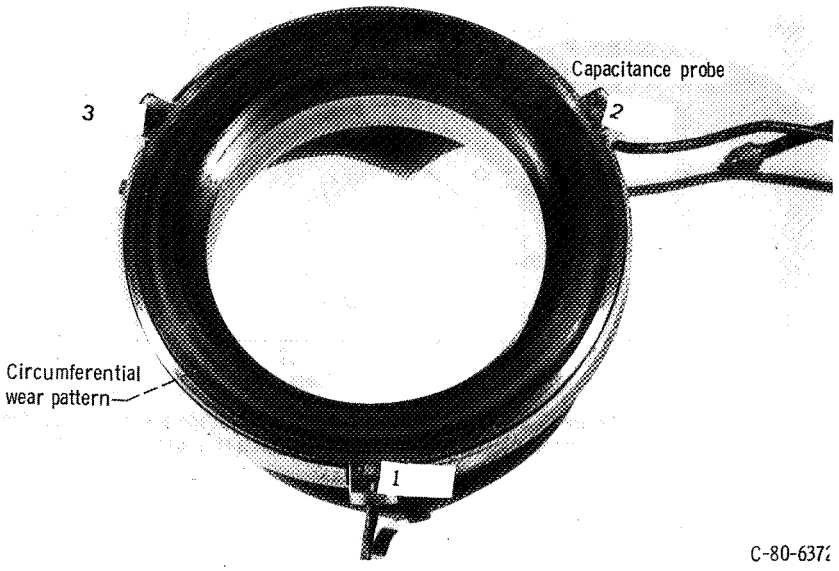

(a) Primary ring, showing wear pattern.

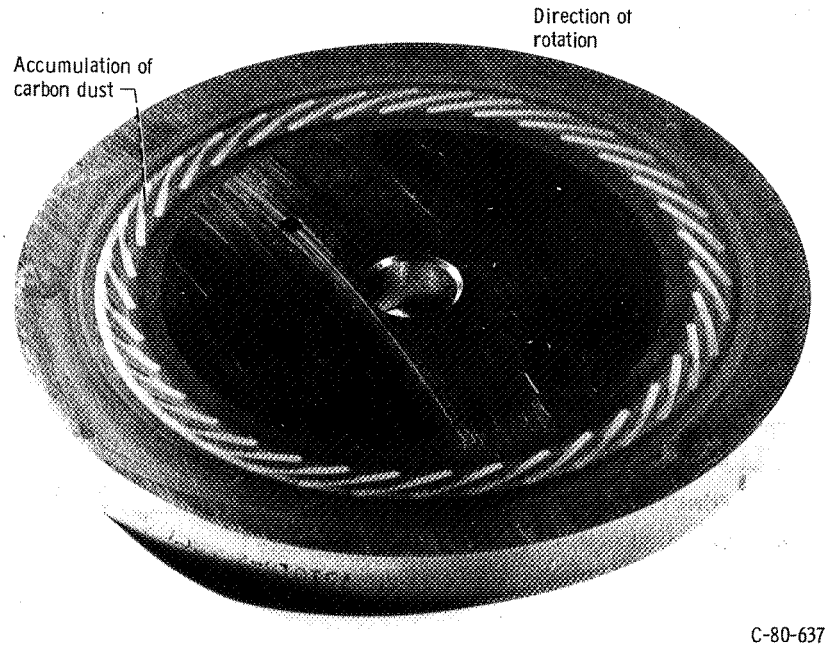

(b) Seat, showing accumulation of carbon dust at outer portion of spiral grooves.

Figure 16. - Outward-pumping spiral groove seal.

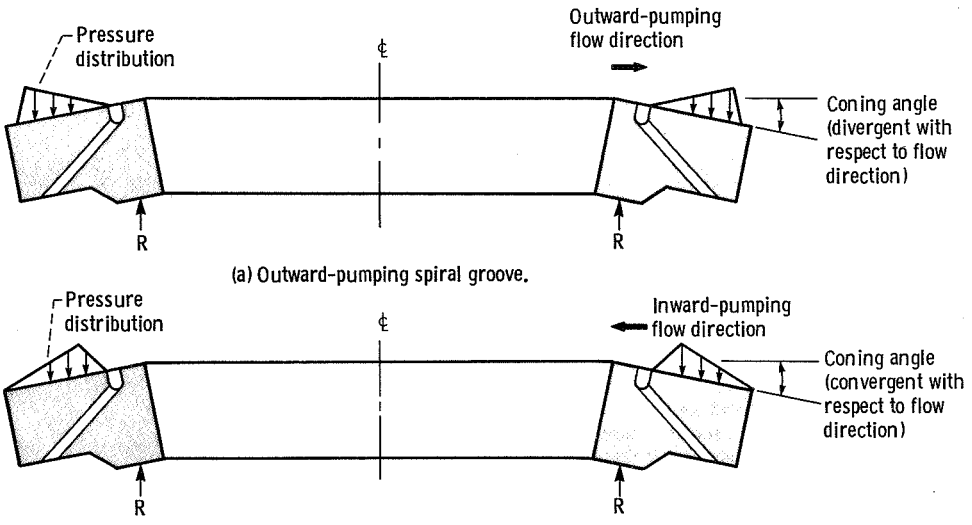

(a) Outward-pumping spiral groove.

(b) Inward-pumping spiral groove.

Figure 17. - Schematics showing coning angles with respect to flow direction.

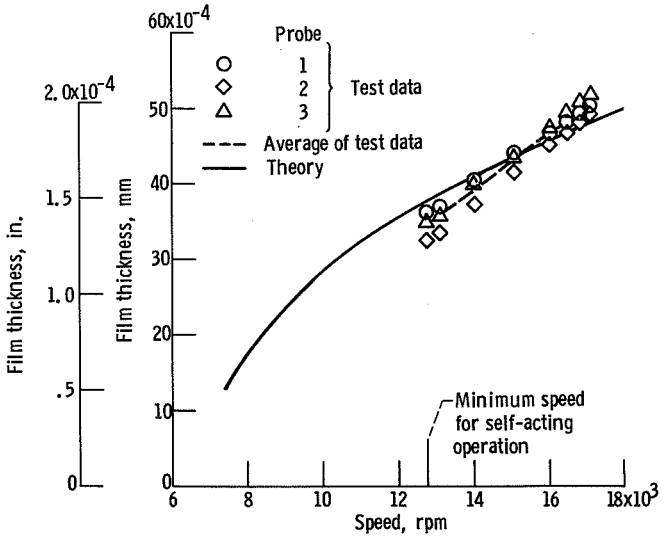

Figure 18. - Film thickness as function of shaft speed - comparison of test data with theory for inward-pumping spiral groove. Groove depth, 0.023 mm (0.0009 in.); seal face load, 73 N (16.4 lb).

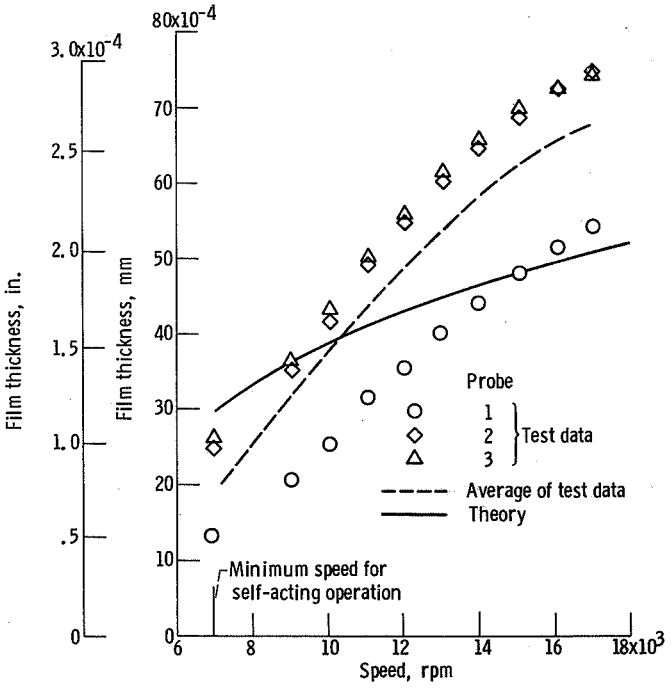

Figure 19. - Film thickness as function of shaft speed - comparison of test data with theory for inward-pumping, shallow spiral groove. Groove depth, 0.015 mm (0.0006 in.); seal face load, 73 N (16.4 lb).

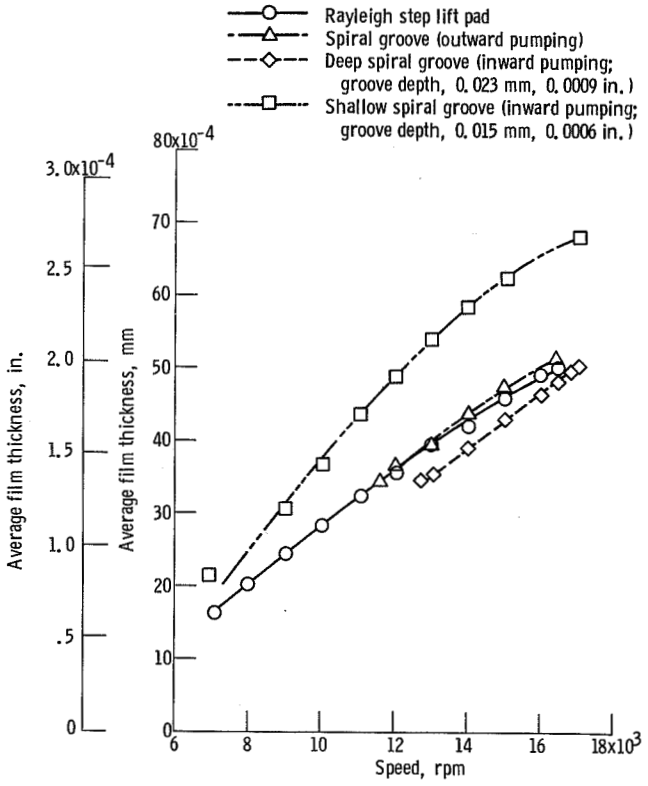

Figure 20. - Average film thickness as function of shaft speed (test data) for Rayleigh step lift pad, outward-pumping spiral groove, and inward-pumping spiral groove face seals. Seal face load, 73 N (16.4 lb).

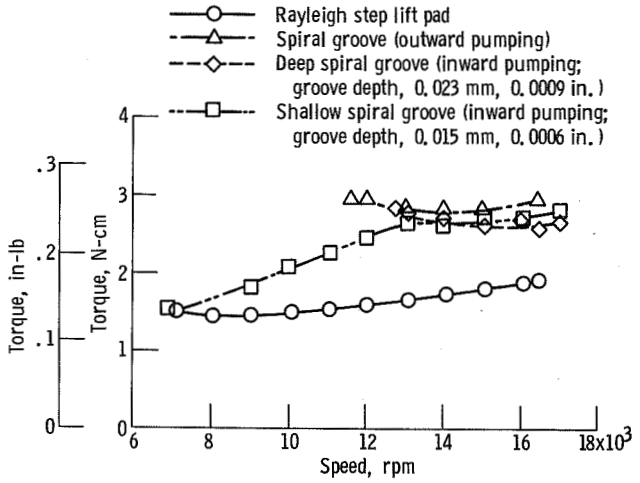

Figure 21. - Seal torque as function of shaft speed (test data) for Rayleigh step lift pad, outward-pumping spiral groove, and inward-pumping spiral groove face seals. Seal face load, 73 N (16.4 lb).

1. Report No.	2. Government Accession No.	3. Recipient's Catalog No.
NASA TP-2058		

4. Title and Subtitle	5. Report Date
FILM THICKNESS MEASUREMENT FOR SPIRAL GROOVE AND RAYLEIGH STEP LIFT PAD SELF-ACTING FACE SEALS	October 1982
	6. Performing Organization Code: 505-32-42
7. Author(s): Eliseo DiRusso	8. Performing Organization Report No.: E-1169
	10. Work Unit No.
9. Performing Organization Name and Address: National Aeronautics and Space Administration, Lewis Research Center, Cleveland, Ohio 44135	11. Contract or Grant No.
	13. Type of Report and Period Covered: Technical Paper
12. Sponsoring Agency Name and Address: National Aeronautics and Space Administration, Washington, D.C. 20546	14. Sponsoring Agency Code

15. Supplementary Notes

16. Abstract

One Rayleigh step lift pad and three spiral groove self-acting face seal configurations were tested to measure film thickness and frictional torque as a function of shaft speed. The seals were tested at a constant face load of 73 N (16.4 lb) with ambient air at room temperature and atmospheric pressure as the fluid medium. The test speed range was from 7000 to 17 000 rpm. The measured film thickness was compared with theoretical data from mathematical models. The mathematical models overpredicted the measured film thickness at the lower speeds of the test speed range and underpredicted the measured film thickness at the higher speeds of the test speed range.

17. Key Words (Suggested by Author(s))	18. Distribution Statement
Seals; Self-acting face seals; Gas film thickness; Spiral groove; Rayleigh step lift pad; Gas bearings	Unclassified - unlimited STAR Category 07

19. Security Classif. (of this report)	20. Security Classif. (of this page)	21. No. of Pages	22. Price*
Unclassified	Unclassified	20	A02

* For sale by the National Technical Information Service, Springfield, Virginia 22161

NASA-Langley, 1982

National Aeronautics and
Space Administration

Washington, D.C.
20546

Official Business
Penalty for Private Use, $300

THIRD-CLASS BULK RATE

Postage and Fees Paid
National Aeronautics and
Space Administration
NASA-451

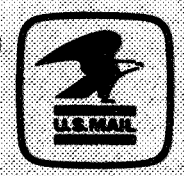

NASA

POSTMASTER: If Undeliverable (Section 158
Postal Manual) Do Not Return